*Journal of Mechanics*, 2022, **38**, 13–21
https://doi.org/10.1093/jom/ufab036
**Regular Article**

# Numerical study of hydrodynamic herringbone-grooved journal bearings combined with thrust bearings considering thermal effects

Chin-Cheng Wang [1,*] and Jyun-Ting Lin [2]

[1]Department of Vehicle Engineering, National Taipei University of Technology, Taipei, Taiwan
[2]Department of Mechanical Engineering, Yuan Ze University, Chung-Li, Taoyuan, Taiwan

*Corresponding author: chincwang@ntut.edu.tw

## ABSTRACT

Hydrodynamic herringbone-grooved journal bearings (HGJBs) are analyzed by solving Navier–Stokes and energy equations. It is well known that the load capacity of hydrodynamic bearings may be affected by high temperatures and low oil viscosity. Therefore, the main objective of this study is to understand the pressure distribution of hydrodynamic HGJBs under different oil viscosity and eccentricity ratios. In this paper, 3 different configurations are studied, namely, a HGJB, a combined HGJB and thrust bearing, and a combined HGJB and grooved thrust bearing. The bearing characteristics, such as load capacity and attitude angle that vary with different eccentricity ratios, are also discussed. The results show that the load capacity of the bearing decreases with increasing temperature. The pressure difference also increases as the eccentricity ratio increases. The high-pressure region is concentrated at the tip of the groove for the HGJB. In addition, the combined HGJB and grooved thrust bearing can be used to stabilize the journal because of the low attitude angle. These findings may help and facilitate the design of hydrodynamic bearings suitable for working in warm and hot environments in the future.

**KEYWORDS:** herringbone-grooved journal bearing, grooved thrust bearing, thermal effect, attitude angle

## NOMENCLATURE

$c$ = radial clearance (mm)
$D$ = journal diameter (mm)
$E$ = total energy (J/kg)
$e$ = eccentricity ratio
$k$ = thermal conductivity (W/m·K)
$L$ = length of journal bearing (mm)
$N$ = rotational speed (rps)
$p$ = pressure (Pa)
$p_{ave}$ = average pressure (Pa)
$R$ = radius of bearing (mm)
$S$ = Sommerfeld number
$T$ = temperature (K)
$\vec{v}$ = velocity vector (m/s)
$\triangle x$ = displacement along $x$-direction (mm)
$\mu$ = dynamic viscosity (kg/m·s)
$\rho$ = density (kg/m$^3$)
$\tau$ = viscous shear (Pa)

## 1. INTRODUCTION

Researchers have generally ignored the effect of lubricating oil temperature, in order to shorten the computational time of numerical simulation of hydrodynamic bearings. However, frictional heat can significantly increase the temperature of the lubricant, thus changing its viscosity. For example, the lubricant of an electronic cooling fan changes its viscosity due to the effect of the ambient temperature. Therefore, its bearing load capacity and performance will also be affected. At high rotational speeds, the viscosity and pressure change considerably due to the increase in the temperature of the lubricant. To predict the characteristics of the hydrodynamic bearing more accurately, it is important to consider the change in lubricant viscosity. Wang and He [1] used computational fluid dynamics to analyze a hydrodynamic journal bearing and a herringbone-grooved journal bearing (HGJB). They found that a herringbone-grooved journal redistributes the high-pressure region to the groove tip. The leakage rate of a herringbone-grooved journal is smaller than a hydrodynamic journal bearing. However, they did not consider the effect of temperature on lubricating oil viscosity. In order to predict the characteristics of the bearing more accurately, we considered the thermal effect of the bearing. Majumdar [2] studied the density of lubricant, which is varied linearly with temperature, and the journal bearing viscosity was a function of temperature. Majumdar compared their results of temperature and pressure distribution with the experimental data of Cole [3]. The conclusion showed the circumferential temperature and pressure distribution are in the same trend. The decrease in pressure was seen in all the loadings using variable properties of lubricant. The variable properties of lubricant lowered the load carrying capacity of the bearing. Banwait and Chandrawat

**Received:** 16 September 2021; **Accepted:** 28 December 2021

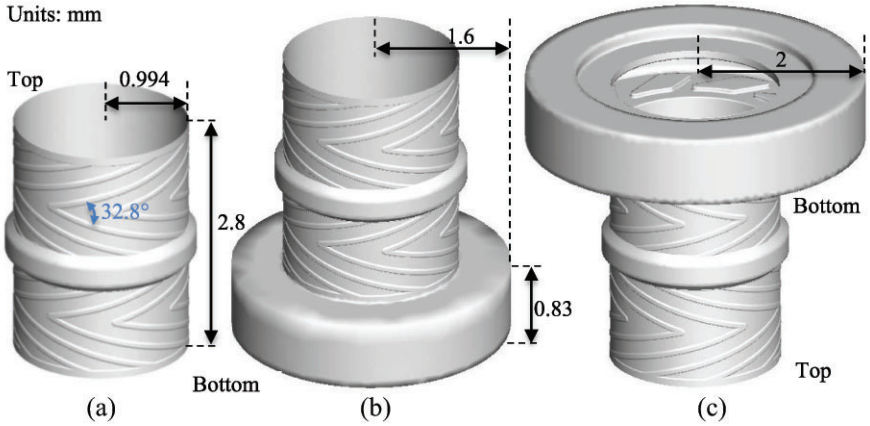


**Figure 1** Schematics of hydrodynamic (a) HGJB, (b) HGJB-TB, and (c) HGJB-GTB.

[4] showed that bush and journal run at higher temperature when they are used at higher speeds under a given load. In addition, when both the eccentricity ratio and the journal speed increase, the maximum bush temperature also increases. A significant effect of thermal distortions of the bush/journal was found. Boubendir *et al.* [5] analyzed the thermo-hydrodynamic self-lubrication of porous circular journal bearing. They found that the effect of temperature on the performance of journal bearings is very important, and the gradual decrease in pressure distribution and load capacity was the result of increased permeability. The higher the permeability, the greater the area of maximum temperature. Gao [6] analyzed the crankshaft of motorcycle engine and solved the Reynolds and energy equations. The results showed that the load capacity of the journal is quite large. However, at a high eccentricity ratio, the bearing will be damaged. As the frictional heat increases, the temperature rises, so the temperature in the high-pressure zone is higher than the temperature in the low-pressure zone. The temperature of the lubricating oil in the high-pressure zone continues to rise until the lubricating oil enters the cavitation zone. The low-temperature lubricant forms a cavitation zone, which cools the high-temperature lubricant. The effect of temperature on viscosity is significant. Sahu *et al.* [7] showed that due to the groove in the shaft, the fluid temperature has a wave-like nature. Due to the higher-pressure distribution, the maximum fluid temperature increases as the eccentricity ratio increases. Compared with a plain journal bearing, a HGJB has a better load carrying capacity and low-end leakage. It has also been observed that the HGJB is more stable than the conventional plain journal bearing. Singh *et al.* [8] solved the Reynolds and energy equations to analyze the thermo-hydrodynamic HGJB problem. They found that the temperature of the fluid film rises due to frictional heat, resulting in a decrease in viscosity and load capacity. When the shaft rotating speed increased, the load capacity and bush temperature also increased. A bearing with smaller groove angles had higher load capacity. The temperature gradient in the radial direction was much larger than the temperature gradient in the circumferential direction. Jang *et al.* [9] investigated the characteristics of the hydrodynamic herringbone-grooved bearing of the hard disk drive (HDD) spindle motor, considering the viscosity of the lubricant due to elevated temperature. They solved the Reynolds and heat conduction equations to investigate the coupling temperature and the characteristics of HDD spindle motor hydrodynamic journal bearings. They found that the load capacity of the bearing will increase due to the rotational speed and surrounding temperature. This research showed that the variation of clearance at elevated temperature is another important design consideration that affects the characteristics of the HDD spindle motor. Yu and Sadeghi [10] investigated the effect of groove geometry on the hydrodynamic lubrication mechanism of thrust washers. They studied the pressure distribution of different groove depths, widths, groove numbers and shapes by solving the Reynolds equation, film thickness equation and force balance equation. They found that for certain operating conditions, thrust washers can support large loads with proper groove geometry. The key to the load support mechanism is the presence of grooves, which can cause pressure to build up in the convergent regions of the grooves.

The purpose of this study is to understand and compare the pressure distribution generated by the hydrodynamic HGJB with and without the installation of the thrust bearing. At the same time, we consider the effect of warm and hot environments on lubricant viscosity and examine eccentricity ratios ranging from 0.1 to 0.6. In the previous literature [1], we have validated the use of 3-dimensional (3D) Navier–Stokes equations to calculate the relationship between the Sommerfeld number and the eccentricity ratio of hydrodynamic bearings. Therefore, in this study, we use the previous method and add the energy equation to discuss the pressure distribution and load capacity of the hydrodynamic HGJB while considering the thermal effect. In addition, grooved and non-grooved thrust bearings are discussed to understand the stability of the hydrodynamic bearing.

## 2. PROBLEM DESCRIPTION

The geometry of hydrodynamic HGJBs with and without thrust bearings used in this study is shown in Fig. 1. The journal radius is 0.994 mm, the bearing radius is 1 mm, the radial clearance is 0.006 mm, the bearing length is 2.8 mm, the groove width is 0.0787 mm, the groove depth is 0.01 mm and the groove angle is 32.8°. The thrust bearing has a radius of 1.6 mm and length

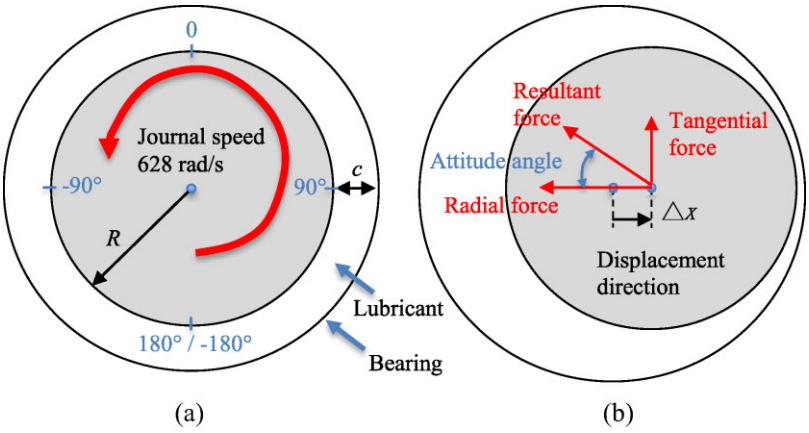


**Figure 2** Top view of hydrodynamic journal bearing (a) without eccentricity and (b) with eccentricity ratio.

of 0.83 mm. The grooved thrust bearing has a radius of 2 mm, length of 0.83 mm, groove width of 0.5 mm and groove depth of 0.05 mm. The bearing eccentricity ratio, $e$, is expressed as: $e = \triangle x/c$, where $\triangle x$ is the centerline displacement and $c$ is the radial clearance shown in Fig. 2. As the eccentricity ratio increases, the minimum clearance is located in the direction of displacement. The Sommerfeld number [11], $S$, is expressed as: $S = (p_{ave}/N\mu)\ (c/R)^2$, where $p_{ave}$ is the average pressure, $N$ is the rotational speed, $\mu$ is the viscosity of lubricant and $R$ is the radius of bearing. The lubricating oil is SAE 10W, with a density of 860 kg/m$^3$, a thermal conductivity of 0.13 W/m·K and specific heat of 2000 J/kg·K. We obtained the viscosity of lubricant from the engineering toolbox [12] and assumed that the viscosity of the lubricant only depends on temperature. We used curve fitting to find the viscosity polynomial based on temperature. Because the density varies slightly with temperature from 20°C to 100°C, there is not much thermal expansion. We assumed the density of lubricant is constant. For a warm environment from 293K to 343K, the polynomial is $\mu(T) = a_1 + a_2T + a_3T^2 + a_4T^3 + a_5T^4$, where the coefficients are $a_1 = -238.549$, $a_2 = 2.986444$, $a_3 = -0.01396278$, $a_4 = 0.0000289106$ and $a_5 = -0.000000022377$. For a hot environment from 344K to 373K, the polynomial is $\mu(T) = b_1 + b_2T + b_3T^2$, where the coefficients are $b_1 = 0.208$, $b_2 = -0.00075$ and $b_3 = 0.00000056$.

## 3. NUMERICAL MODEL

SAE 10W oil is the lubricant used in this study and is generally considered to be an incompressible viscous fluid. Since the clearance between the journal and the bearing is 6 mm, the flow condition is laminar. The maximum Reynolds number under the given conditions is much less than 50, and gravity and energy generation are neglected. For an incompressible Newtonian fluid, the steady-state continuity, momentum and energy equations are given as follows:

$$\nabla \cdot \vec{v} = 0 \tag{1}$$

$$\rho(\vec{v} \cdot \nabla)\vec{v} = -\nabla p + \mu\nabla^2\vec{v} \tag{2}$$

$$\nabla \cdot [\vec{v}(\rho E + p)] = \nabla \cdot [k\nabla T + (\tau \cdot \vec{v})] \tag{3}$$

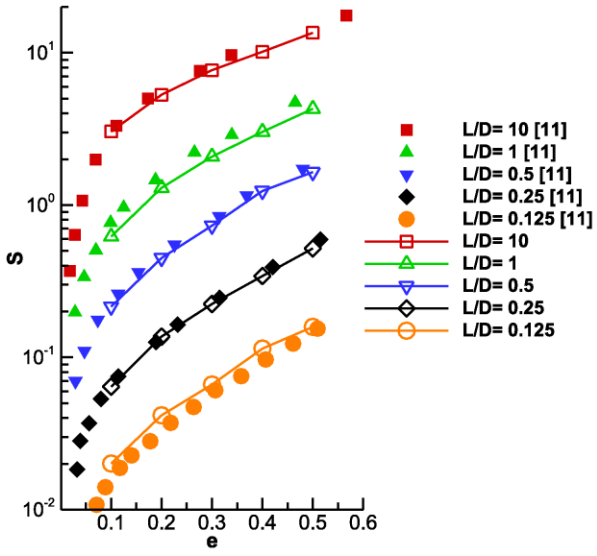


**Figure 3** Benchmark validation of Sommerfeld number versus eccentricity ratio and the ratio of journal bearing length to its diameter (L/D).

where $\vec{v}$ is velocity vectors in 3 dimensions, $p$ is pressure, $E$ is the total energy, $k$ is the thermal conductivity and $\tau$ is viscous tensor.

We validated our numerical results of journal bearing geometry with published values of Sommerfeld number versus eccentricity ratio [11], shown in Fig. 3. The published curves were computed using the Reynolds boundary condition, which is more accurate. For practical engineering applications, a value of Sommerfeld number for a specific eccentricity and L/D ratio and then the bearing and operating parameters can be selected to give an optimum performance. Higher values of eccentricity ratio are prone to shaft misalignment difficulties; lower values may cause shaft vibration and are associated with higher friction and lubricant temperature. Our numerical results were in good agreement with the published data.

We repeated the calculations using coarse, medium and fine grids. The convergence of the residuals of all discrete conservation equations was less than $10^{-4}$ for all cases. The circumferential velocity along the radial clearance from the

**Table 1** The boundary conditions for all 3 configurations.

| Configuration | HGJB | HGJB-TB | HGJB-GTB |
|---|---|---|---|
| Top | 1 atm/293K or 363K | 1 atm/293K or 363K | 1 atm/293K or 363K |
| Bottom | Fixed wall/adiabatic | Fixed wall/adiabatic | Fixed wall/adiabatic |
| Inner journal | Moving wall/adiabatic | Moving wall/adiabatic | Moving wall/adiabatic |
| Outer bearing | Fixed wall/343K or 373K | Fixed wall/343K or 373K | Fixed wall/343K or 373K |

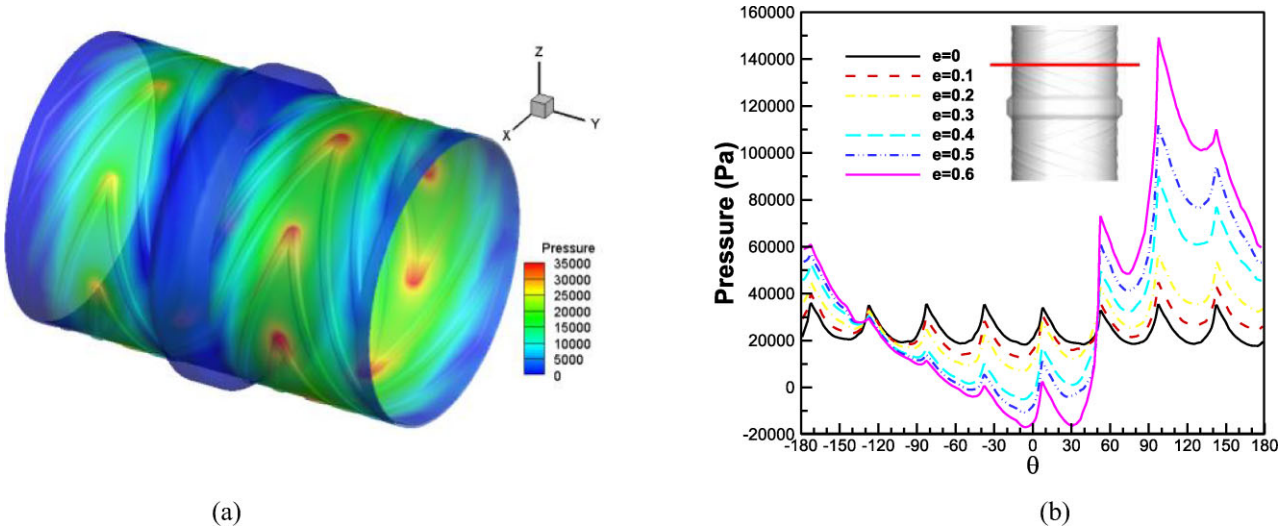


**Figure 4** Pressure distribution of HGJB in a warm environment for (a) 3D orientation without eccentricity and (b) along the groove tip (i.e. red line) with different eccentricity ratios in the azimuthal direction.

coarse grid to the fine grid is less than 2%. Thus, the medium grid is chosen. For the mesh of a hydrodynamic HGJB, we tested 3 different grids with 750 000, 1 840 000 and 3 140 000 cells. The solution was found to be grid independent when the grid size exceeded 1 840 000 cells. Therefore, in order to reduce the computation time, 1 840 000 cells were chosen as our computational mesh. Similarly, for a HGJB with a thrust bearing (HGJB-TB) and a HGJB with a grooved thrust bearing (HGJB-GTB), grid sizes of 2 300 000 and 2 500 000 cells were selected for the computational meshes. The computing facility has 12 cores with two Intel Xeon E5-2620 CPUs (2 GHz) and 64 GB of DDR3-1600 memory. Convergence criteria were satisfied when the residuals of all discrete conservation equations were less than a chosen value of $10^{-4}$. Each case took approximately 2 hours running in parallel to converge.

Three configurations were considered in the present study, including a hydrodynamic HGJB, HGJB-TB, and HGJB-GTB. The viscosity of SAE 10W oil depends on the temperature in warm (i.e. below 343 K) and hot (i.e. above 363 K) environments. The boundary conditions for the 3 configurations are shown in Table 1. For all cases, a moving wall rotational speed of 628 rad/s was applied at the inner journal. For the outer bearing and bottom boundaries, no-slip boundary conditions were assumed. For the top boundary, a zero-gauge pressure outlet condition is employed.

## 4. RESULTS AND DISCUSSION

Fig. 4a shows the pressure contour of the hydrodynamic HGJB without eccentricity in a warm environment. The results show that the peak pressure appeared at the tip of the herringbone groove because the static pressure reaches its maximum at the stagnation point. The advantage of these herringbone grooves is that they give higher load capacity. Next, the relationship between eccentricity ratio and pressure was examined. Fig. 4b shows the circumferential pressure distribution along the groove tip when the eccentricity ratio was 0 to 0.6 in a warm environment. When the journal moves in the direction of $\theta = 90°$, the fluid flow experiences converging and diverging regions, generating hydrodynamic pressure. That is why the pressure will rise and then fall when the pressure is close to 90°. When the eccentricity ratio increased, the peak pressure increased. For an eccentricity ratio of 0.6, the peak pressure rose to a maximum at an angle of approximately 100°. Fig. 5a shows the pressure contour of the HGJB without eccentricity in a hot environment. A similar pressure distribution trend could be observed. However, the pressure difference observed in a hot environment was much lower than that in a warm environment. This is because the viscosity of lubricant is low in a hot environment. Fig. 5b shows the maximum pressure increase due to an increase in the eccentricity ratio. As the eccentricity ratio increased, the high-pressure peak was concentrated at the tip of a groove. However, the maximum pressure was about half that in a warm environment.

Fig. 6a shows the pressure contour of the HGJB-TB without eccentricity in a warm environment. A thrust bearing can be used to handle thrust load on one side. The results showed that the pressure near the bottom of the thrust bearing was lower than the pressure at the top of the HGJB-TB because of its symmetrical design. The peak pressure occurred at the tip of the groove

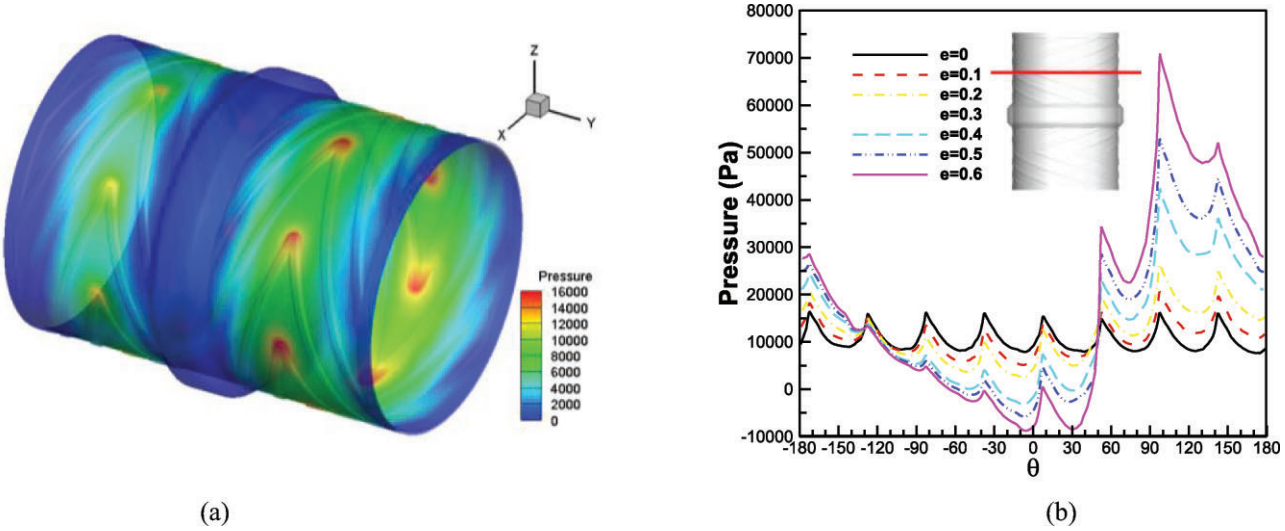


**Figure 5** Pressure distribution of HGJB in a hot environment for (a) 3D orientation without eccentricity and (b) along the groove tip (i.e. red line) with different eccentricity ratios in the azimuthal direction.

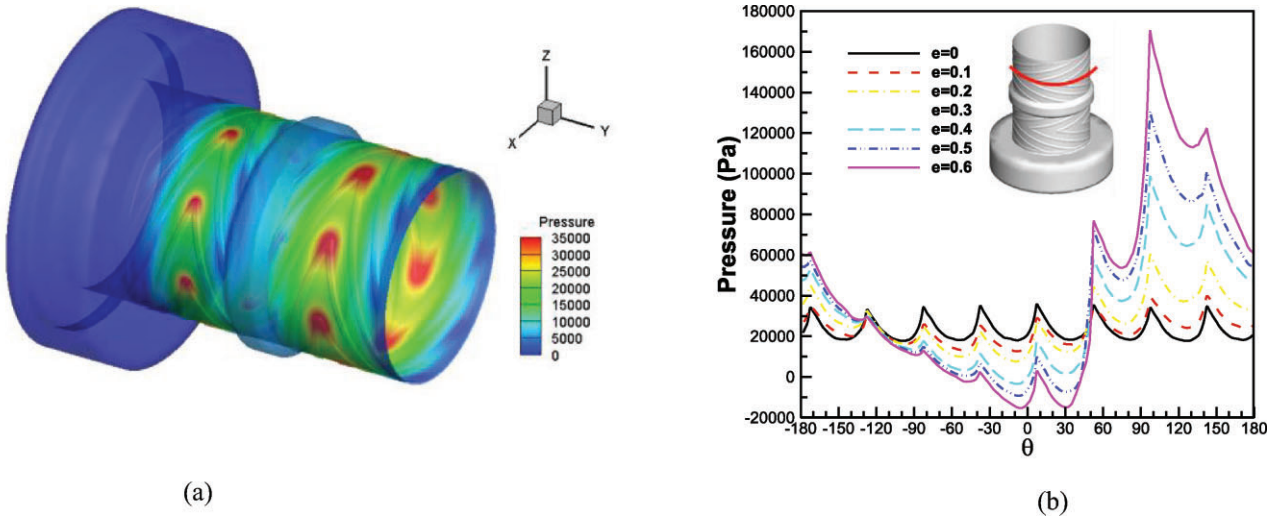


**Figure 6** Pressure distribution of HGJB-TB in a warm environment for (a) 3D orientation without eccentricity and (b) along the groove tip (i.e. red line) with different eccentricity ratios in the azimuthal direction.

due to the stagnation pressure. Fig. 6b shows the circumferential pressure distribution along the groove tip when the eccentricity ratio is 0 to 0.6. In a warm environment, the pressure distribution trend of the HGJB-TB is similar to that of the HGJB. The results showed that the peak pressure is concentrated at the tip of the groove and increased with an increase in the eccentricity ratio. The increase in pressure is due to the viscous lubricant is dragged into the converging clearance by the moving surface. Fig. 7a shows the pressure contour of the HGJB-TB in a hot environment. Due to the low viscosity at high temperatures, the peak pressure was about half of that in a warm environment. Fig. 7b shows the circumferential pressure distribution along the groove tip when the eccentricity ratio was 0 to 0.6 in a hot environment. The peak pressure increased as the eccentricity ratio increased.

Fig. 8a shows the pressure contour of the HGJB-GTB without eccentricity in a warm environment. The grooved thrust bearing includes a number of pads arranged in a circle around the journal. These form wedge-shaped lubricant regions of inside the HGJB-GTB, which support the applied thrust. The results show that the pressure distribution was similar to the HGJB and the HGJB-TB. Fig. 8b shows the pressure distribution of the HGJB-GTB at the cross-section of the bottom-grooved thrust bearing. The high and low peaks of each wedge-shaped groove could be found. In addition, the average pressure at the top of the grooved thrust bearing was higher than the average pressure at the bottom of the bearing. Fig. 9a shows the pressure contour of the HGJB-GTB without eccentricity in a hot environment. A similar trend was observed in the pressure distribution in warm and hot environments. Fig. 9b shows the pressure distribution of the HGJB-GTB at the cross-section of the bottom-grooved thrust bearing. The peak pressure difference between the high and low peak of each wedge-shaped groove is almost half of that in a warm environment. To understand the pressure difference between the top and bottom of a grooved thrust bearing, we

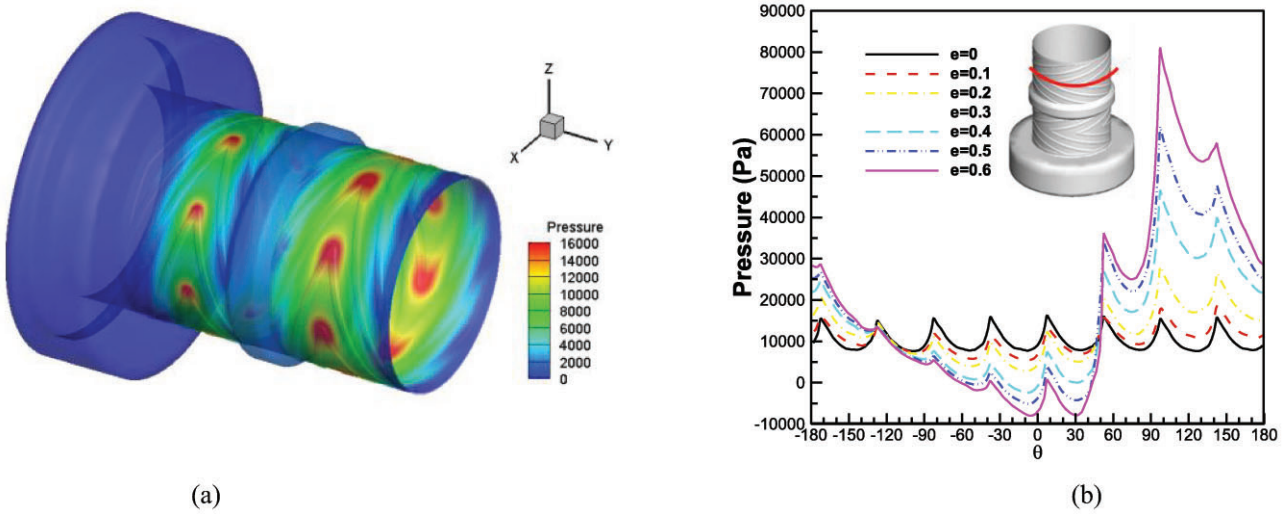


**Figure 7** Pressure distribution of HGJB-TB in a hot environment for (a) 3D orientation without eccentricity and (b) along the groove tip (i.e. red line) with different eccentricity ratios in the azimuthal direction.

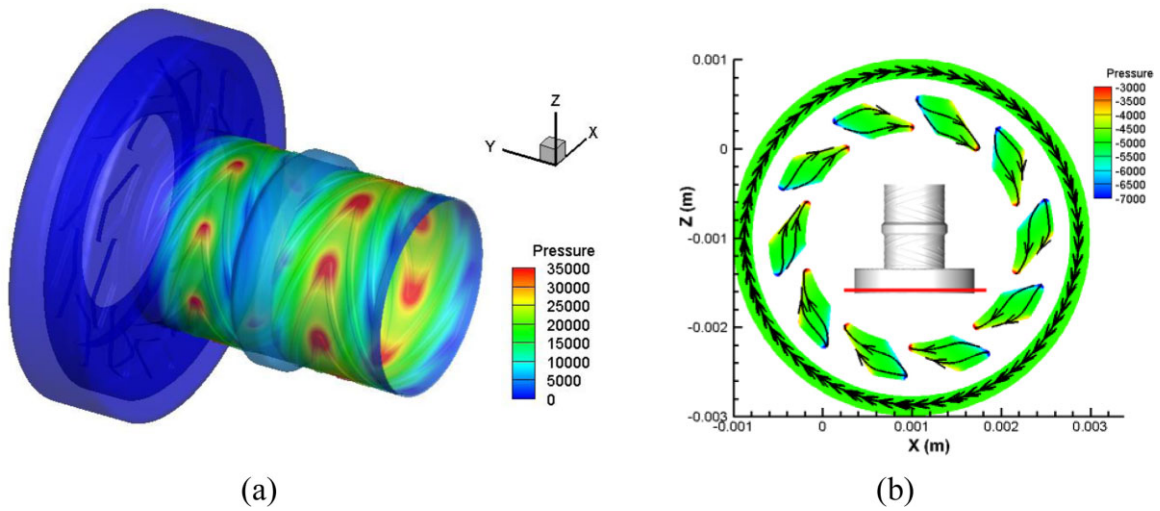


**Figure 8** Pressure distribution of HGJB-GTB without eccentricity in a warm environment for (a) 3D orientation and (b) 2-dimensional (2D) cross-section at the bottom of grooved thrust bearing (i.e. red line).

observed the axial pressure distribution from the corner of the top rectangular groove to the corner of the bottom rectangular groove in warm and hot environments. The results show that the pressure at the top corner was higher than the pressure at the bottom corner. The peak pressure difference was lower in a hot environment than in a warm environment. This pressure difference can stabilize the journal to the grooved thrust bearing.

Fig. 10a shows a comparison of the circumferential pressure distribution without eccentricity in a warm environment for all 3 configurations. All 3 configurations show very similar pressure distribution trends. The peak pressure occurred at the tip of the groove in all cases. The peak pressure in the HGJB-GTB was the highest of all 3 configurations because the grooved thrust bearing provided additional load capacity. Fig. 10b shows a comparison of the circumferential pressure distribution without eccentricity in a hot environment for all 3 configurations. The results show that in warm and hot environments, the pressure distribution tended to be very similar. However, the peak pressure in a hot environment was almost half of that in a warm environment because the lubricant had low viscosity in a hot environment. Fig. 11 shows a comparison of the circumferential pressure distribution with an eccentricity ratio of 0.3 in warm and hot environments for all 3 configurations. The results show that the peak pressure in the HGJB-GTB was higher than the other two configurations. When the eccentricity ratio was 0.6, the same phenomenon could be found, as shown in Fig. 12. Tables 2 and 3 show the relationship between the eccentricity ratio, radial force, tangential force and attitude angle of all 3 configurations in warm and hot environments. We can see that for all 3 configurations, the attitude angles with an eccentricity ratio of 0.3 were higher than those with an eccentricity ratio of 0.6. The lower attitude angle indicates that the hydrodynamic journal bearing had higher stability. It can be seen that the attitude angle of the HGJB-GTB was the smallest among all

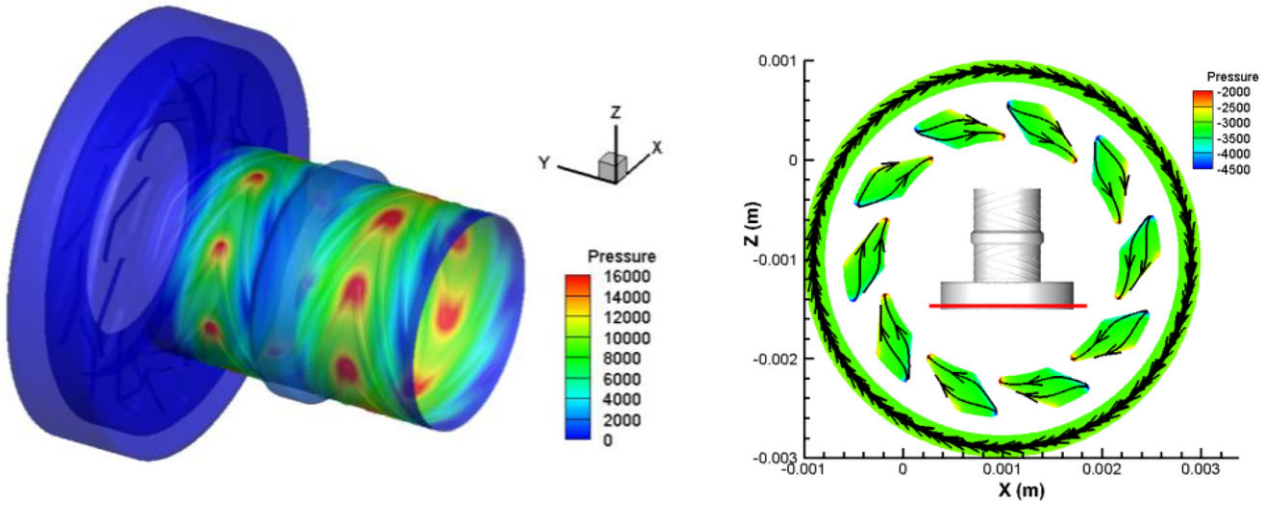


**Figure 9** Pressure distribution of HGJB-GTB without eccentricity in a hot environment for (a) 3D orientation and (b) 2D cross-section at the bottom of grooved thrust bearing (i.e. red line).

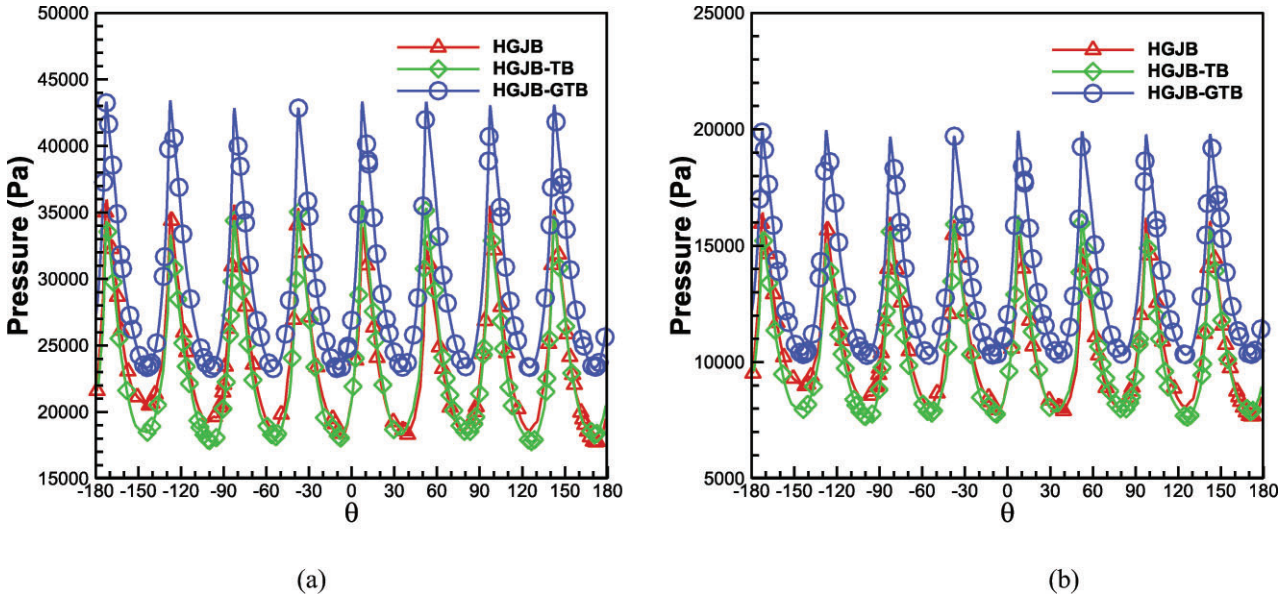


**Figure 10** Comparison of circumferential pressure distribution of all 3 configurations without eccentricity in (a) warm and (b) hot environments.

**Table 2** Relationship between eccentricity ratio, radial force, tangential force and attitude angle in a warm environment for all 3 configurations.

| Configuration | HGJB | HGJB-TB | HGJB-GTB |
|---|---|---|---|
| Eccentricity | 0.3/0.6 | 0.3/0.6 | 0.3/0.6 |
| Radial force (N) | 0.0376/0.0966 | 0.0521/0.134 | 0.066/0.165 |
| Tangential force (N) | 0.135/0.294 | 0.0812/0.194 | 0.0903/0.212 |
| Attitude angle | 74.4°/71.8° | 57.3°/55.4° | 53.9°/52.2° |

**Table 3** Relationship between eccentricity ratio, radial force, tangential force and attitude angle in a hot environment for all 3 configurations.

| Configuration | HGJB | HGJB-TB | HGJB-GTB |
|---|---|---|---|
| Eccentricity | 0.3/0.6 | 0.3/0.6 | 0.3/0.6 |
| Radial force (N) | 0.0179/0.0462 | 0.0249/0.0642 | 0.0316/0.0807 |
| Tangential force (N) | 0.0646/0.141 | 0.0389/0.0929 | 0.0432/0.104 |
| Attitude angle | 74.5°/71.9° | 57.4°/55.4° | 53.9°/52.3° |

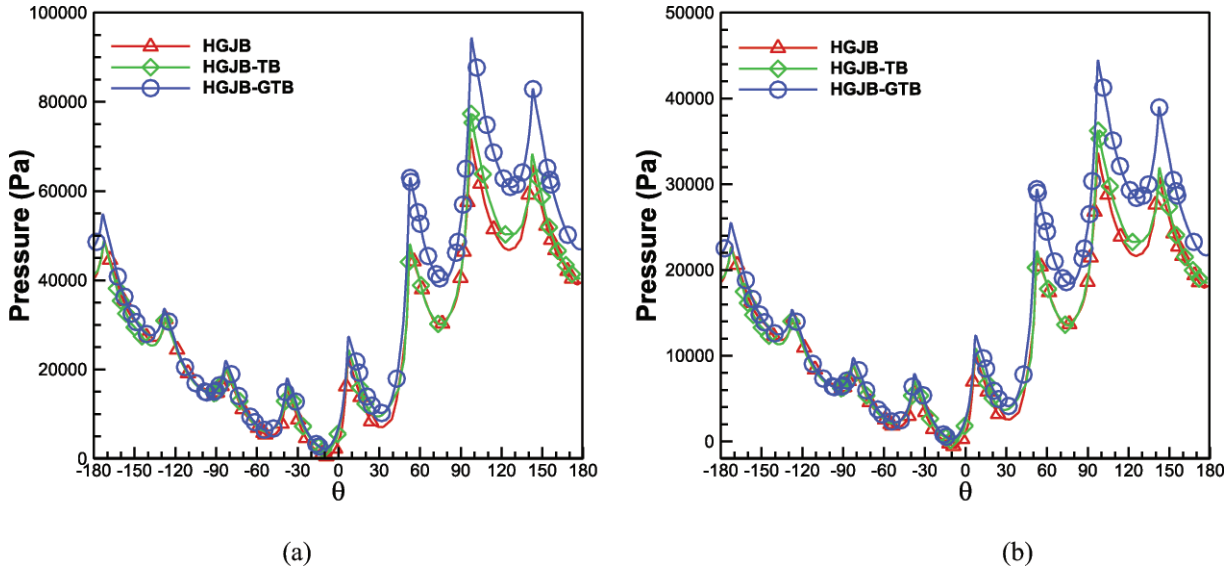


**Figure 11** Comparison of circumferential pressure distribution of all 3 configurations for eccentricity ratio of 0.3 in (a) warm and (b) hot environments.

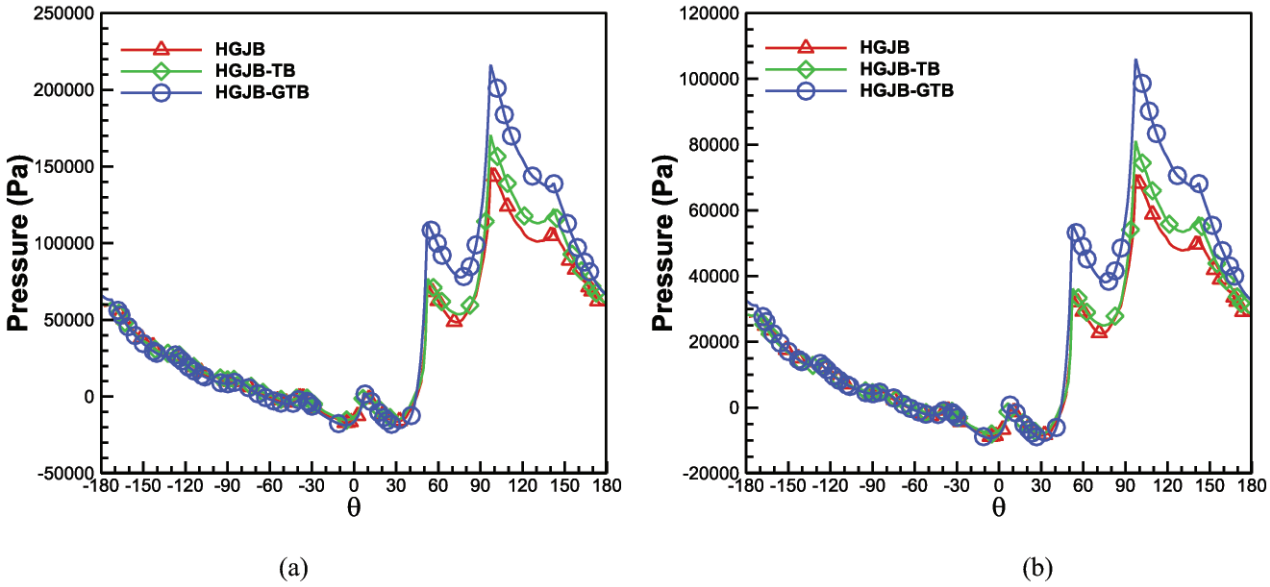


**Figure 12** Comparison of circumferential pressure distribution of all 3 configurations for eccentricity ratio of 0.6 in (a) warm and (b) hot environments.

3 configurations. Therefore, the HGJB-GTB was the most stable hydrodynamic bearing design.

## 5. CONCLUSIONS

The main objective of this study was to investigate thermal effects on the performance of a HGJB, HGJB-TB, and HGJB-GTB. The 3D Navier–Stokes equations and the energy equation are solved by the finite volume method. The numerical results of journal bearing are verified and validated by conducting a grid independence study and comparing with published data. The average pressure of the HGJB is related to temperature because the viscosity is affected by temperature. A low viscosity reduces the average pressure in a hot environment. As the eccentricity ratio increases, the pressure difference increases significantly. For the HGJB without eccentricity, high pressure is generated at the tip of the groove. When the eccentricity ratio increases, the peak pressure increases and is concentrated in the vicinity of the eccentricity direction. A comparison of circumferential pressure distribution shows that the peak pressure of the HGJB-GTB is greater than the other two configurations. When the eccentricity ratio increases, the peak pressure increases. The advantage of the HGJB is that the high-pressure zone and low-pressure zone is redistributed, thereby avoiding the cavitation effect. In addition, the peak pressure at the tip of the groove stabilizes and the journal is kept in the center of the bearing. The attitude angle is lower

in the HGJB-GTB than the HGJB-TB and the HGJB. In a warm environment, the average pressure and the maximum pressure are higher than those in a hot environment. For example, the maximum peak pressure of the HGJB-TB with an eccentricity ratio of 0.3 in a warm environment is approximately 76 000 Pa, and the maximum peak pressure in a hot environment is approximately 36 000 Pa. The bearing load capacity is the integral of the pressure. Therefore, the bearing load capacity in a warm environment is higher than that in a hot environment. To generalize our numerical findings, we found that when we increase the temperature from 20 degrees to 100 degrees, the pressure field at any point in a warm environment is almost twice that of a hot environment. When we increased the eccentricity ratio from 0.3 to 0.6, the maximum pressure difference was doubled. Lower operating temperature and higher eccentricity ratio can improve the performance of hydrodynamic journal bearings.

## ACKNOWLEDGEMENTS

The authors were supported by the Tung Pei Industrial Co., Ltd.

## REFERENCES

1. Wang C-C, He C-L. Numerical study of a hydrodynamic journal bearing with herringbone grooves for oil leakage reduction. *Proceedings of the Institution of Mechanical Engineers, Part J: Journal of Engineering Tribology* 2019;**233**(3):439–446.
2. Majumdar BC. The thermohydrodynamic solution of oil journal bearings. *Wear* 1975;**31**(2):287–294.
3. Cole JA. An experimental investigation of temperature effects in journal bearings. *Proceedings of the Convention on Lubrication and Wear, Institution of Mechanical Engineers, London* 1957;**111**: 111–117.
4. Banwait SS, Chandrawat HN. Study of thermal boundary conditions for a plain journal bearing. *Tribology International* 1998;**31**(6):289–296.
5. Boubendir S, Larbi S, Bennacer R. Numerical study of the thermo-hydrodynamic lubrication phenomena in porous journal bearings. *Tribology International* 2011;**44**(1):1–8.
6. Gao YS. *Analysis of journal bearings under consideration of varying loading and squeezed film*. M.S. thesis, National Taiwan University, Taiwan, 2008.
7. Sahu M, Sarangi M, Majumdar BC. Thermo-hydrodynamic analysis of herringbone grooved journal bearings. *Tribology International* 2006;**39**(11):1395–1404.
8. Singh U, Roy L, Sahu M. Steady-state thermo-hydrodynamic analysis of cylindrical fluid film journal bearing with an axial groove. *Tribology International* 2008;**41**(12):1135–1144.
9. Jang GH, Kim KS, Lee HS, Kim CS. Analysis of a hydrodynamic bearing of a HDD spindle motor at elevated temperature. *Journal of Tribology* 2004;**126**(2):353–359.
10. Yu TH, Sadeghi F. Groove effects on thrust washer lubrication." *Journal of Tribology* 2001;**123**(2):295–304.
11. Stachowiak G, Batchelor AW. *Engineering Tribology*. Oxford: Butterworth-Heinemann, 2013, 150–153.
12. Motor oil - dynamic viscosities. https://www.engineeringtoolbox.com/dynamic-viscosity-motor-oils-d_1759.html.